Unconventional fabrication of 2D nanostructures and graphene edges

Bellunato, A.

CHAPTER 6

Transverse nanogaps from the layered assembly of polyelectrolytes

Molecular transistors, electromagnetic waveguides and quantum tunnelling junctions comprise precisely separated nanogaps of nanometric and subnanometric spacing. Nonetheless, fabricating a nanogap remains a technological challenge, particularly using approaches such as breakdown electromigration and lithography. Hereby, nanogaps are templated via microtomy of metallic thin films embedded in a polymer matrix and precisely separated by a nanometric, sacrificial layer of polyelectrolytes grown via Layer-by-Layer (LbL) deposition. The versatility of the LbL technique, both in terms of number of layers and composition of polyelectrolytes, allows to finely tune the spacing across the gap. Further, microtomy converts such films into nanogaps transferrable on arbitrary substrates. Ultimately, reactive plasma etches the sacrificial layers of polyelectrolytes, effectively opening the gap. These findings pave the path towards molecularly defined nanogaps of high precision and stability, modular into complex architectures for the next generation of devices integrating nanogap components.

Publication in preparation: Amedeo Bellunato, Clarisse de Sere, Zhanna Overchenko, Bram Koster, Sai Sankar Gupta, Pauline van Deursen and Grégory F. Schneider.

6.1 Introduction

Solid state nanogaps interface bulky electrodes at nanometric distance either as in plane nanogaps or in the form of molecular break junctions. The precise control of the spacing across a nanogap is critical for the design of such architectures and their application into tunnelling junctions[1–4], molecular transistors[3,5–8] and waveguides[9–13]. For instance, the characteristics of devices such as molecular transistors rely on the specific molecular structure of the bridging element, and most importantly require electrodes separated by a gap having a width comparable to the one of a single molecule[14], i.e. a few nanometres. Similarly, tunnelling junctions are based on electrodes separated by a few nanometres, across which the tunnelling current flowing between the electrodes has been used to detect[15] or study electronic transport through single molecules[16–19]. Nonetheless, the precise, controllable fabrication of nanogaps still challenges the limits of conventional lithography. While innovative strategies have been developed to achieve precisely aligned electrodes[20,21], several drawbacks remain, mainly the stability of the gap with temperature[22,23] and the presence of particles detrimental for the performances of the gap[24]. Alternatively, sacrificial layers have been used to separate the metallic electrodes using organic or inorganic frameworks which are – in a later step – selectively etched yielding an empty gap spacing[25–27].

In this chapter, the Layer-by-Layer deposition[28], LbL, is used to grow multilayered films of polyelectrolytes of discrete thicknesses between large area metallic thin films, subsequently embedded into a polymeric matrix and converted by microtomy into molecular nanogaps spaced by a sacrificial film of polyelectrolytes. Microtomy was first introduced by Whitesides and co-workers as an unconventional approach towards the reliable and serial production of metallic nanostructures and nanoelectrodes[29–31]. Here, a diamond knife transversally slices the polymer matrix and the metallic thin films, yielding thin slabs of polymer surrounding a gold-polyelectrolytes-gold nanogap. Next, the molecular nanogap opens using plasma reactive etching of the sacrificial polyelectrolytes, emptying the spacing across the gap. The polymeric support allows the manipulation of such nanostructures, their precise alignment and the assembly into complex architectures. For instance, by precisely transferring two consecutive slabs on

porous substrates, we could assemble nanopores devices, impossible otherwise, by overlapping two twisted nanogaps[32,33].

The multilayered film is grown by simple alternate dipping of the substrate into aqueous solutions of oppositely charged polyelectrolytes. The growth is self-limited and governed by electrostatic interactions between the polyelectrolyte layers. The effective charge of the polyelectrolytes in solution can be controlled by modulating the ionic strength of the solvent, namely the concentration of the salt in solution during deposition, through counter ion screening[34]. Particularly, with polyelectrolytes such as poly (allylamine hydrochloride) (PAH) and poly (sodium 4-styrenesulfonate) (PSS), each layers within the stratified film can have a thickness varying between 0.25-2.2 nm in aqueous solutions of NaCl with concentration varying from 0.015 M[35] to 2M[34]. The temperature and the humidity during the deposition can also modulate the compactness of the layers composing the films, resulting in thinner polyelectrolytes films at higher temperatures (and lower humidity), due to a lower water content within the multilayered film[36]. Thus, multilayered films of polyelectrolytes yield nanometric thin films with possibility to control the film thickness down to a nanometer, allowing to design polyelectrolyte-nanogap architectures with tunable gap size in the nanometer range.

6.2 Results and discussion

The multilayered spacers are grown via Layer-by-Layer deposition (LbL) of alternatively charged polyelectrolytes between large area metallic thin films. Next, microtomy slices nanometric thin sections of the metallic thin films by means of an ultra-sharp diamond knife. The diamond knife cuts the metallic films into parallel pairs of nanorods forming a nanogap, which gap is filled with multilayered polyelectrolytes. Reactive ion etching removes the polyelectrolytes, emptying the space across the gap, and yielding nanogaps composed of precisely separated metallic nanorods.

The mechanical cut performed during microtomy requires a strong adhesion of the multilayered polyelectrolytes to the metallic thin films, in order to preserve the architecture of the nanogap between nanorods. While the multilayered polyelectrolytes are bound together via electrostatic interactions between the individual polyelectrolytes layers, the first metallic film must be functionalized in order to attract and bind the first layer of polyelectrolytes. Therefore, a gold thin

film was deposited over a supporting substrate (i.e. SiO_2) and functionalized with a mixed self-assembled-monolayer (SAM) of amino and alkyl-thiols assembled from a solution of 5 mM 1-dodecanethiol and 5 mM 1-amino 11-undecanethiol in ethanol[37] (respectively what we refer to as alkyl thiols and aminothiols), Figure 6.1a.

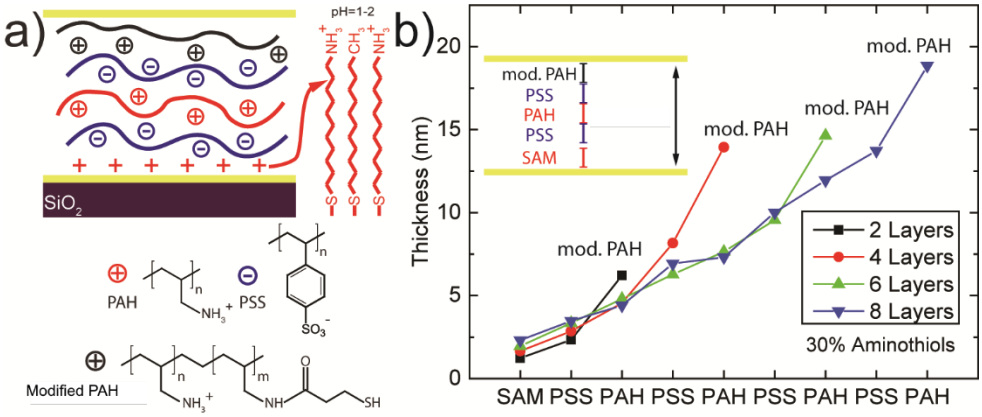

Figure 6.1. Multilayered polyelectrolytes-nanogap. a) Alternated Layer-by-Layer deposition of poly (sodium 4-styrenesulfonate) and poly (allylamine hydrochloride) in between two large area (1 X 1 cm^2) gold layers to form a multilayered nanogap. The first gold layer is functionalized with a mixed self-assembled monolayer of amino-thiols and alkyl-thiols formed from a solution of 5 mM 1-dodecanethiol and 5 mM 1-amino 11-undecanethiol in ethanol at a 7:3 volume ratio. The top layer of polyelectrolytes is a poly (allylamine hydrochloride) layer derivatized with thiols (see Figure IV.2 appendix IV). b) Characterization of the growth of the multilayered polyelectrolytes by ellipsometry.

Next, the thiolated gold film was immersed into an acidic solution of PSS at pH= 1-2. The amines of the aminothiol are protonated favouring the adsorption of a layer of negatively charged PSS[28], Figure 6.1a. Then, the multilayered spacer is grown via alternated dipping of the substrate in an aqueous solution of PSS and PAH in 1M KCl. Finally, the multilayered polyelectrolytes are coated with a second gold film deposited via thermal resistance evaporation. In order to promote the adhesion between the multilayered polyelectrolytes and the top gold film, the outmost layer of polyelectrolytes is chemically functionalized. To do so, the amines of the outmost PAH layer are partially converted into thiol groups which seal to the gold through thiols bonds (see Figure 6.2 appendix IV). When immersed in KCl solution, the residual amines of the thiolated PAH (i.e. modified PAH in Figure 6.1a) drive

the deposition over the multilayered film of polyelectrolytes, while the thiols bind the gold film, Figure 6.1a.

The thickness of the multilayered film grows linearly, around 1.5 +/- 0.1 nm per layer. The last partially thiolated PAH layer is around 5 +/- 0.3 nm thick, due to the lower content of amines on its backbone, Figure 6.1b. In fact, the adsorption of polyelectrolytes depends on electrostatic interactions and charge screening. As a result, each layer adsorbs until the charge of the previous layer is compensated, with polyelectrolyte residual groups providing a charge overcompensation. Since the last thiolated PAH possesses a lower amines content compared to the pristine PAH, a thicker film was obtained: a higher amount of polyelectrolyte chain is required to screen effectively the negative charge in the previous PSS layer.

In order to process the multilayered nanogap by microtomy, the gold films are embedded within a polymer scaffold (Figure 6.2a) composed of a mixture of pentaerythritoltetrakis mercaptopropionate (PEMPT), and triallyl triazinetrione (TATATO) with a 3:4 molar proportion and cured under UV irradiation at 532 nm for half an hour (see materials and methods in Appendix IV). Next, a diamond knife slices the polymer scaffold via microtomy, forming nanometric polymeric slabs 150 nm thick embedding a nanogap comprising two gold nanorods spaced by a multilayered polyelectrolyte film (Figure 6.2b). The polymer frame mechanically supports the nanogap and allows the facile transfer of the slices from the diamond knife to a support substrate. Finally, reactive O_2 plasma etching removes the sacrificial film of polyelectrolytes and (for longer exposures) the supporting polymer, yielding a planar nanogap across metallic nanorods (Figure 6.2c).

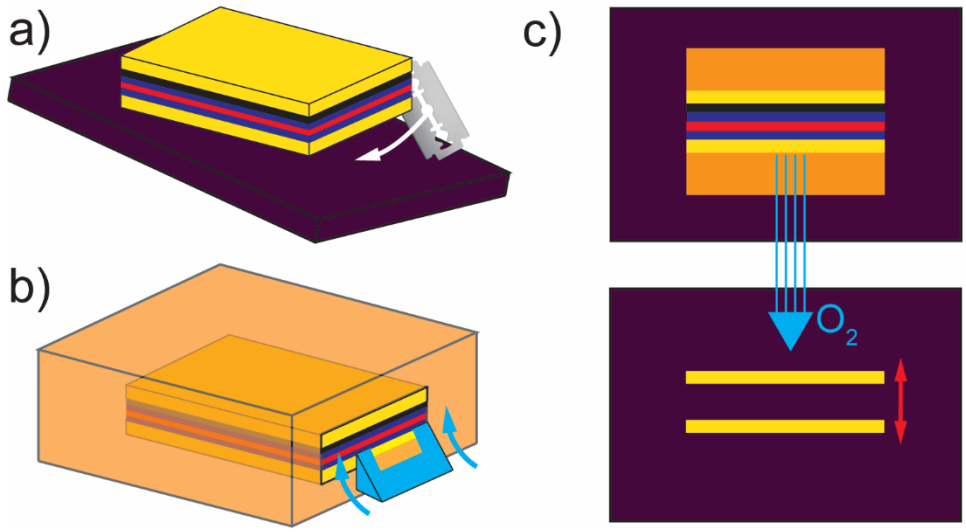

Figure 6.2. Illustration of the transverse microtomy of the multilayered nanogap and subsequent formation of an empty nanogap between two gold electrodes. a) The multilayered film of polyelectrolytes is coated with a second layer of gold. The stack is lifted from the substrate by intercalating a razor blade between the gold film and the substrate. The stack is then embedded inside a polymer matrix composed of pentaerythritoltetrakis mercaptopropionate (PEMPT), and triallyl triazinetrione (TATATO) in molar ratio 3 : 4. b) Microtomy of the polymer matrix yielding a nanogap supported by a polymer slab. c) The slab is deposited on a substrate (Si/SiO_2, transmission electron microscope grid, glass) and oxidized using an O_2 plasma to etch both the PEMPT/TATATO polymer and the sacrificial layer of polyelectrolytes, yielding the formation of the nanogap.

The presence of the supporting polymer matrix and the multilayered film of polyelectrolytes prevents the nanogap to shrink during microtomy, therefore permitting the subsequent transfer of the multilayered nanogap to an arbitrary substrate, such as Si/SiO_2 wafers, transmission electron microscope (TEM) grids or SiN membranes (Figure 6.3a and Figure 6.3b). In fact, after microtomy, the slabs slide from the diamond knife to an air-water meniscus placed behind the blade. Next, a perfect loop (i.e. a titanium ring of 1 mm in diameter) is positioned on the water surface surrounding the polymeric slabs. The ring exploits the surface tension of the water to withdraw a droplet of water containing the floating polymeric slabs. The perfect loop allows the transfer of the droplet onto any target substrate, while the water slowly evaporates landing the nanogap over a surface. The slow evaporation of the water gives time to precisely align the slab

over the substrate, using a needle connected to a micro-step manipulator pinning the polymer slab and controlling its position.

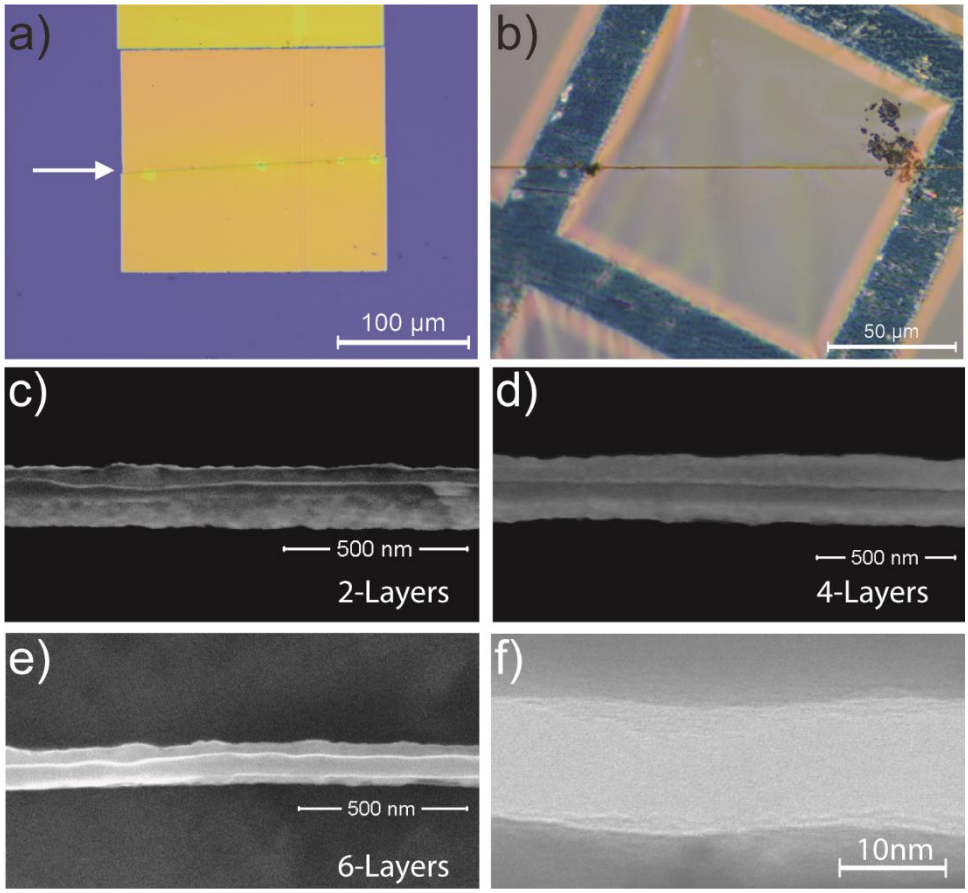

Figure 6.3. Optical and electron microscopy characterization of supported metallic nanogaps. a) Optical micrograph of a PEMPT/TATATO slab (yellow) on a Si/SiO_2 wafer (purple). The position of the gold/polyelectrolytes/gold stack is pointed by the white arrow. b) Optical micrograph of a polymer slab and gold/polyelectrolytes/gold stack supported by a holey TEM grid. c), d) and e) SEM micrographs of molecular nanogaps of two, four and six layers of polyelectrolytes transferred on a Si/SiO_2. f) TEM micrograph of a nanogap formed by four layers of polyelectrolytes.

Figure 6.3c to Figure 6.3e show the scanning electron microscope, SEM, micrographs of a multilayered nanogap on SiO_2 composed respectively of two (Figure 6.3c), four (Figure 6.3d) and six (Figure 6.3e) layers of polyelectrolytes, with thicknesses varying from 5 nm to 15 nm (thicknesses determined by ellipsometry).

Figure 6.3f shows the transmission electron micrograph of a multilayered nanogap composed of four polyelectrolytes layers film of polyelectrolytes. The multilayered film was etched via O_2 plasma prior to imaging, yielding a high contrast in the transmission electron microscopy micrograph (Figure 6.3f) between the empty space of the gap (white area) and the gold nanorods (darker regions at the upper and lower boundaries of the image). TEM allows the high-resolution imaging across the gap, which size, in the order of 10 nm, matches the measurements performed by ellipsometry (Figure 6.1b).

6.3 Conclusions

To conclude, multilayered polyelectrolytes adsorb via Layer-by-Layer deposition between large area gold films further converted into multilayered nanogaps using microtomy. Advantageously, multilayered polyelectrolytes assemble by simple immersion of a substrate in aqueous solutions of polyelectrolytes, forming organic thin films which thickness can be readily monitored by optical methods such as ellipsometry. The chemical functionalization of the gold substrate with self-assembled monolayers and the chemical synthesis of a thiolated PAH ensure the strong adhesion of the multilayered polyelectrolytes to the gold films during microtomy. The mechanical sectioning via microtomy yields multilayered nanogaps embedded within nanometric polymeric supports, allowing the facile handling of the nanogap samples, which are precisely transferrable on discrete target substrates. Specifically, the transfer using a perfect loop and the further alignment allow for the precise control of the position of the nanogap over the substrate, with the possibility of assembling larger (and more complex) architectures by stacking layers of transverse nanogaps on top of each other. For instance, nanopores with sub 10 nm pores can be assembled at the crossing interface of two twisted nanogaps, where the long range nanorods would directly function as nanofluidic injection channels towards the rim of the pore, as we show in Chapter 7[32]. Furthermore, metallic nanorods can be employed as in-situ electrodes for the electrical characterization of the nanogaps, either in the form of tunnelling junctions or molecular transistors.

6.4 References

(1) Reed, M. A. *Science* **1997**, *278* (5336), 252–254.

(2) Huang, S.; He, J.; Chang, S.; Zhang, P.; Liang, F.; Li, S.; Tuchband, M.; Fuhrmann, A.; Ros, R.; Lindsay, S. *Nat. Nanotechnol.* **2010**, *5* (12), 868–873.

(3) Liang, X.; Chou, S. Y. *Nano Lett.* **2008**, *8* (5), 1472–1476.

(4) Fanget, A.; Traversi, F.; Khlybov, S.; Granjon, P.; Magrez, A.; Forró, L.; Radenovic, A. *Nano Lett.* **2014**, *14* (1), 244–249.

(5) Li, T.; Hu, W.; Zhu, D. *Adv. Mat.* **2010**, 22(2), 286–300.

(6) Hwang, J. S.; Kong, K. J.; Ahn, D.; Lee, G. S.; Ahn, D. J.; Hwang, S. W. *Appl. Phys. Lett.* **2002**, *81* (6), 1134–1136.

(7) Kyu Kim, S.; Cho, H.; Park, H.-J.; Kwon, D.; Min Lee, J.; Hyun Chung, B. *Nanotechnology* **2009**, *20* (45), 455502.

(8) Porath, D.; Bezryadin, A.; de Vries, S.; Dekker, C. *Nature* **2000**, *403* (6770), 635–638.

(9) Ward, D. R.; Hüser, F.; Pauly, F.; Cuevas, J. C.; Natelson, D. *Nat. Nanotechnol.* **2010**, *5* (10), 732–736.

(10) Wu, H.-Y.; Choi, C. J.; Cunningham, B. T. *Small* **2012**, *8* (18), 2878–2885.

(11) Chen, X.; Ciracì, C.; Smith, D. R.; Oh, S.-H. *Nano Lett.* **2015**, *15* (1), 107–113.

(12) Marqués-González, S.; Matsushita, R.; Kiguchi, M. *J. Opt.* **2015**, *17* (11), 114001.

(13) Siegfried, T.; Ekinci, Y.; Martin, O. J. F.; Sigg, H. *Nano Lett.* **2013**, *13* (11), 5449–5453.

(14) Perrin, M. L.; Burzurí, E.; Van Der Zant, H. S. J. *Chem. Soc. Rev* **2015**, *44* (44), 835–1030.

(15) Tsutsui, M.; Taniguchi, M.; Yokota, K.; Kawai, T. *Nat. Nanotechnol.* **2010**, *5* (4), 286–290.

(16) Perrin, M. L.; Verzijl, C. J. O.; Martin, C. A.; Shaikh, A. J.; Eelkema, R.; Van Esch, J. H.; Van Ruitenbeek, J. M.; Thijssen, J. M.; Van Der Zant, H. S. J.; Dulić,

D. *Nat. Nanotechnol.* **2013**, *8* (4), 282–287.

(17) Martin, C. A.; Smit, R. H. M.; van der Zant, H. S. J.; van Ruitenbeek, J. M. *Nano Lett.* **2009**, *9* (8), 2940–2945.

(18) Martin, C. A.; Ding, D.; Van Der Zant, H. S. J.; Van Ruitenbeek, J. M. *New J. Phys.* **2008**, *10* (6), 065008.

(19) Martin, C. A.; Ding, D.; Sørensen, J. K.; Bjørnholm, T.; van Ruitenbeek, J. M.; van der Zant, H. S. J. *J. Am. Chem. Soc.* **2008**, *130* (40), 13198–13199.

(20) Park, H.; Lim, A. K. L.; Alivisatos, A. P.; Park, J.; McEuen, P. L. *Appl. Phys. Lett.* **1999**, *75* (1999), 301–303.

(21) Lambert, M. F.; Goffman, M. F.; Bourgoin, J. P.; Hesto, P. *Nanotechnology* **2003**, *14* (7), 772–777.

(22) Danvers E. Johnston; Douglas R. Strachan; A. T. Charlie Johnson, Nano Lett., **2007**, 7 (9), 2774–2777.

(23) Esen, G.; Fuhrer, M. S. *Appl. Phys. Lett.* **2005**, *87* (26), 263101.

(24) Thiti Taychatanapat; Kirill I. Bolotin; Ferdinand Kuemmeth; Ralph, D. C. *Nano Lett.*, **2007**, 7 (3), 652–656.

(25) Zaretski, A.; Marin, B. C.; Moetazedi, H.; Dill, T. J.; Jibril, L.; Kong, C.; Tao, A. R.; Lipomi, D. J. *Nano Lett.* **2015**, *15* (1), 635–640.

(26) Fursina, A.; Lee, S.; Sofin, R. G. S.; Shvets, I. V.; Natelson, D. *Appl. Phys. Lett.* **2008**, *92* (11), 113102.

(27) Zhou, Z.; Zhao, Z.; Yu, Y.; Ai, B.; Mohwald, H.; Chiechi, R. C.; Yang, J. K. W.; Zhang, G. *Adv. Mater.* **2016**, *28* (15), 2956–2963.

(28) Decher, G. *Science.* **1997**, *277* (5330), 1232–1237.

(29) Lipomi, D. J.; Martinez, R. V; Whitesides, G. M. *Angew. Chem. Int. Ed. Engl.* **2011**, *50* (37), 8566–8583.

(30) Storm, a J.; Chen, J. H.; Ling, X. S.; Zandbergen, H. W.; Dekker, C. *Nat. Mater.* **2003**, *2* (8), 537–540.

(31) Carlotti, M.; Degen, M.; Zhang, Y.; Chiechi, R. C. *J. Phys. Chem. C* **2016**, *120* (36), 20437–20445.

(32) Arjmandi-Tash, H.; Bellunato, A.; Wen, C.; Olsthoorn, R. C.; Scheicher, R. H.; Zhang, S.-L.; Schneider, G. F. *Adv. Mater.* **2018**, 1703602.

(33) Bellunato, A.; Vrbica, S. D.; Sabater, C.; de Vos, E. W.; Fermin, R.; Kanneworff, K. N.; Galli, F.; van Ruitenbeek, J. M.; Schneider, G. F. *Nano Lett.* **2018**, *18* (4), 2505–2510.

(34) Decher, G.; Schmitt, J. In *Trends in Colloid and Interface Science VI*, **1992**, 160–164.

(35) Elżbieciak-Wodka, M.; Warszyński, P. *Electrochim. Acta* **2013**, *104*, 348–357.

(36) Decher, G.; Schlenoff, J. *Multilayer Thin Films: Sequential Assembly of Nanocomposite Materials, 2nd Edition*; Wiley-VCH, **2012**; Vol. 1.

(37) Love, J. C.; Estroff, L. A.; Kriebel, J. K.; Nuzzo, R. G.; Whitesides, G. M. *Chem. Rev.* **2005**, *105* (4), 1103–1169.